NUMERICAL STUDY OF MIXED CONVECTION HEAT TRANSFER IN LID-DRIVEN CAVITY UTILIZING NANOFLUID
Effect of Type and Model of Nanofluid

by

Nader POURMAHMOUD, Ashkan GHAFOURI*, and Iraj MIRZAEE

Department of Mechanical Engineering, Urmia University, Urmia, Iran

Original scientific paper
DOI:10.2298/TSCI120718053P

Numerical investigation of the laminar mixed convection in 2-D lid driven cavity filled with water-Al_2O_3, water-Cu or water-TiO_2 nanofluids is done in this work. In the present study, the top and bottom horizontal walls are thermally insulated while the vertical walls are kept at constant but different temperatures. The governing equations are given in term of the stream function-vorticity formulation in the non-dimensionalized form and then solved numerically by second-order central difference scheme. The thermal conductivity and effective viscosity of nanofluid have been calculated by Maxwell-Garnett and Brinkman models, respectively. An excellent agreement between the current work and previously published data on the basis of special cases are found. The governing parameters are Rayleigh number $10^3 \le Ra \le 10^6$ and solid concentration $0 \le \varphi \le 0.2$ at constant Reynolds and Prandtl numbers. An increase in mean Nusselt number is found as the volume fraction of nanoparticles increases for the whole range of Rayleigh numbers. In addition, it is found that significant heat transfer enhancement can be obtained by increasing thermal conductivity coefficient of additive particles. At $Ra = 1.75 \cdot 10^5$, the Nusselt number increases by about 21% for TiO_2-water, and almost 25% for Al_2O_3-water, and finally around 40% for Cu-water nanofluid. Therefore, the highest values are obtained when using Cu nanoparticles. The result obtained using variable thermal conductivity and variable viscosity models are also compared to the results acquired by the Maxwell--Garnett and the Brinkman model.

Key words: *nanofluid, mixed convection, heat transfer, lid-driven cavity, Rayleigh number, solid volume fraction*

Introduction

The main restriction of common fluids used for heat transfer application such as water, ethylene glycol, mineral oil or propylene glycol is their low thermal conductivity. Nanofluid, which is a mixture of nano-size particles suspended in base fluid, has a superior thermal conductivity compared to the base fluid. Due to their potential in enhancement of heat transfer, nanofluids have attracted enormous interest for researchers and artisans such that many researchers have investigated different aspects of nanofluids [1]. Eastman *et al.* [2], in their experimental work, showed that an increase in thermal conductivity of nearly 60% could be obtained for a nanofluid considering of water and 0.05 solid volume fraction CuO nanoparticles. Lee *et al.* [3] measured the thermal conductivity of Al_2O_3-water and Cu-water nanoflu-

* Corresponding author; e-mail: a.ghafouri@urmia.ac.ir

ids and demonstrated that the thermal conductivity of nanofluids increases with solid volume fraction. Das *et al.* [4] expressed 2-4-times increase in thermal conductivity enhancement for water-based nanofluids containing Al_2O_3 or CuO nanoparticles. Various models for estimating thermal conductivity developed that mostly focused on several parameters such as temperature, size, and shape of nanoparticles, Brownian motion, mean path of fluid particles, *etc.* Maxwell [5] proposed a model to predict the thermal conductivity of low dense mixture that contains solid particles. Several other models have been proposed for calculating the effective thermal conductivity of solid-fluid system Maxwell-Garnet [6], Bruggeman [7], Hamilton and Crosser [8], Wasp [9], Yu and Choi [10], Petal *et al.* [11], and Chon *et al.* [12]. Since the very small nanoparticles are added to the base fluid, nanofluids as single phase flows have been considered [5]. Furthermore, various viscosity correlations such as Brinkman [13], Nguyen *et al.* [14], Pak and Cho [15], *etc.*, have been developed for several nanofluids [16, 17].

Fluid flow and heat transfer in 2-D square cavity driven by buoyancy and shear have been studied extensively in the literature [18-22]. Mixed convection in lid-driven cavity flow problems are encountered in variety of thermal engineering application including cooling of electronic devices, multi-shield structures used for nuclear reactors, furnaces, lubrication technologies, chemical processing equipment, food processing, high-performance building insulation, glass production, solar power collectors, drying technologies, etc [23]. Arpaci and Larson [24] have presented an analytical treatment of the mixed convection heat transfer in cavity, which had one vertical side moving, vertical boundaries at different temperatures, and horizontal boundaries adiabatic. A review on numerical studied reveals that they can be classified into two groups as the following: the first one is denoted as mixed convection in pure base fluid concerned with horizontal top or bottom wall or both walls sliding lid driven cavities, in which the walls have a constant velocity [25-27] or oscillating [28, 29] and another walls are maintained at different constant temperatures while upper and bottom walls are thermally insulated. Any other rotation in the boundary conditions in this group can be considered [30]. The second group of numerical investigations particularly deals with mixed convection flows in a lid-driven square cavity utilizing nanofluid. Tiwari and Das [21] numerically investigated the heat transfer augmentation in a lid-driven cavity filled with nanofluid. They found that the presence of nanoparticles in a base fluid is capable of increasing the heat transfer capacity of the base fluid. Chamkha and Abu-Nada [31] focused on the flow in single and double-lid square cavity filled with a water-Al_2O_3 nanofluid. Two viscosity models are used, namely, Brinkman [13] and Pak and Cho [15] correlation. Their results showed that a significant heat transfer enhancement could be obtained by increasing the nanoparticle volume fractions at moderate and large Richardson number using both nanofluid models. Talebi *et al.* [32] investigated the laminar mixed convection flow through a copper-water nanofluid in a square lid-driven cavity. They found that at fixed Reynolds number, the solid concentration effects on the flow pattern and thermal behavior particularly for higher Rayleigh number. Also their results showed that the effect of solid concentration decreases by the increase of Reynolds number. Muthtamilselvan *et al.* [33] reported on the heat transfer enhancement of copper-water nanofluids in a lid-driven enclosure with different aspect ratios.

The main motivation of this study is to investigate the mixed convection heat transfer in lid-driven cavity utilized with nanofluids. Three different nanoparticles as Al_2O_3, Cu, and TiO_2 and also two variable viscosity and thermal conductivity models are used to study the effect of nanoparticles on mixed convection flow and temperature fields and also comprehensive study on the change of type and used model of nanofluid along with other parameters determining the flow pattern is performed. In the present study, the stream function-vorticity

formulation has been applied for simulation the flow feature of nanofluids and the results will be obtained for a wide range of Rayleigh number and volume fraction of solid particles (φ).

Problem description

Figure 1 depicts schematics of the 2-D lid-driven cavity considered in this paper. The fluid in the cavity is a water-based nanofluid containing different type of nanoparticles Cu, Al_2O_3, and TiO_2. The nanofluid is assumed as incompressible and the flow is assumed to be laminar. It is supposed that the base fluid (*i. e.* water) and the nanoparticles are in thermal equilibrium and no slip occurs between them. The shape and the size of solid particles are furthermore assumed to be uniform and their diameter to be equal to 100 nm. The top and bottom horizontal walls are thermally insulated while the vertical walls are kept at constant but different temperatures. In order to induce the buoyancy effect, the left vertical wall is kept at a relatively high temperature (T_H) and right vertical wall is maintained at a relatively low temperature (T_C). Top wall slides from left to right with uniform velocity. The thermo-physical properties of the pure water and the nanofluid at temperature of 25 °C are given in tab. 1. The thermo-physical properties of the nanofluid are assumed to be constant except for the density variation, which is approximated by the Boussinesq model.

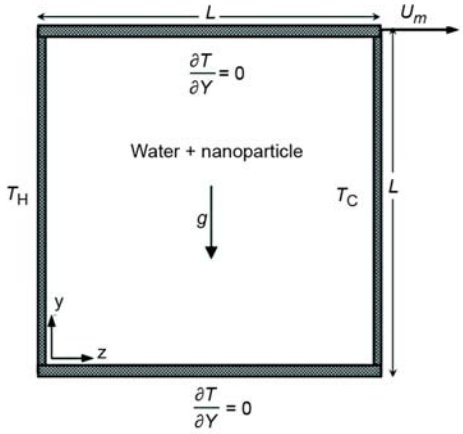

Figure 1. Schematic of problem

Table 1. Thermo-physical properties of fluid and nanoparticles

Physical properties	Fluid phase (water)	Cu	Al_2O_3	TiO_2
C_p [Jkg^{-1}K^{-1}]	4179	383	765	686.2
ρ [kgm^{-3}]	997.1	8933	3970	4250
k [Wm^{-1}K^{-1}]	0.613	400	25	8.95
$\beta\times10^{-5}$ [K^{-1}]	21	1.67	0.85	0.9

Mathematical formulation

The steady-state equations that govern the conservation of mass, momentum, and energy can be written in non-dimensional forms:

$$\frac{\partial U}{\partial X} + \frac{\partial V}{\partial Y} = 0 \tag{1}$$

$$U\frac{\partial U}{\partial X} + V\frac{\partial U}{\partial Y} = -\frac{\partial P}{\partial X} + \frac{1}{\mathrm{Re}}\frac{\mu_{\mathrm{nf}}}{\rho_{\mathrm{nf}}\nu_{\mathrm{f}}}\left(\frac{\partial^2 U}{\partial X^2} + \frac{\partial^2 U}{\partial Y^2}\right) \tag{2}$$

$$U\frac{\partial V}{\partial X} + V\frac{\partial V}{\partial Y} = -\frac{\partial P}{\partial Y} + \frac{\mu_{\mathrm{nf}}}{\rho_{\mathrm{nf}}\nu_{\mathrm{f}}}\frac{1}{\mathrm{Re}}\left(\frac{\partial^2 V}{\partial X^2} + \frac{\partial^2 V}{\partial Y^2}\right) + \frac{(\rho\beta)_{\mathrm{nf}}}{\rho_{\mathrm{nf}}\beta_{\mathrm{f}}}\frac{\mathrm{Ra}}{\mathrm{Pr}\,\mathrm{Re}^2}\theta \tag{3}$$

$$U\frac{\partial \theta}{\partial X} + V\frac{\partial \theta}{\partial Y} = \frac{\alpha_{\mathrm{nf}}}{\alpha_{\mathrm{f}}}\frac{1}{\mathrm{Re}\,\mathrm{Pr}}\left(\frac{\partial^2 \theta}{\partial X^2} + \frac{\partial^2 \theta}{\partial Y^2}\right) \tag{4}$$

In eqs. (1)-(4), the following non-dimensional parameters are used:

$$X=\frac{x}{L},\quad Y=\frac{y}{L},\quad U=\frac{u}{U_m},\quad V=\frac{v}{U_m},\quad P=\frac{p}{\rho_{\mathrm{nf}}U_m{}^2},\quad \theta=\frac{T-T_{\mathrm{C}}}{T_{\mathrm{H}}-T_{\mathrm{C}}},$$
$$\mathrm{Re}=\frac{U_mL}{\nu_{\mathrm{f}}},\quad \mathrm{Pr}=\frac{\nu_{\mathrm{f}}}{\alpha_{\mathrm{f}}},\quad \mathrm{Gr}=\frac{g\beta L^3(T_{\mathrm{H}}-T_{\mathrm{C}})}{\nu_{\mathrm{f}}{}^2},\quad \mathrm{Ra}=\mathrm{Gr}\,\mathrm{Pr},\quad \mathrm{Ri}=\frac{\mathrm{Gr}}{\mathrm{Re}^2} \tag{5}$$

The viscosity of the nanofluid can be approximated as viscosity of the base fluid (μ_{f}) containing dilute suspension of fine spherical particles. In the current study, two models are used to model the viscosity of the nanofluids, which are the Brinkman [13] model and the Pak and Cho [15] correlation. Main results of this study are based on Brinkman [13] model and effect of second model is expressed in the final results at the end of the article. The Brinkman [13] model defined:

$$\frac{\mu_{\mathrm{nf}}}{\mu_{\mathrm{f}}}=\frac{1}{(1-\varphi)^{2.5}} \tag{6}$$

The effective density of the nanofluid at the reference temperature is:

$$\rho_{\mathrm{nf}}=(1-\varphi)\rho_{\mathrm{f}}+\varphi\rho_{\mathrm{s}} \tag{7}$$

and the heat capacitance of nanofluid is:

$$(\rho C_{\mathrm{p}})_{\mathrm{nf}}=(1-\varphi)(\rho C_{\mathrm{p}})_{\mathrm{f}}+\varphi(\rho C_{\mathrm{p}})_{\mathrm{s}} \tag{8}$$

As given by Xuan and Li [34], also the effective thermal conductivity of the nanofluid is approximated by the Maxwell-Garnett [6] model:

$$\frac{k_{\mathrm{nf}}}{k_{\mathrm{f}}}=\frac{k_{\mathrm{s}}+2k_{\mathrm{f}}-2\varphi(k_{\mathrm{f}}-k_{\mathrm{s}})}{k_{\mathrm{s}}+2k_{\mathrm{f}}+\varphi(k_{\mathrm{f}}-k_{\mathrm{s}})} \tag{9}$$

In term of the stream function-vorticity formulation, the governing equations are:

$$\frac{\partial^2\Psi}{\partial X^2}+\frac{\partial^2\Psi}{\partial Y^2}=-\Omega \tag{10}$$

$$U\frac{\partial\Omega}{\partial X}+V\frac{\partial\Omega}{\partial Y}=\frac{\dfrac{\mu_{\mathrm{nf}}}{\mu_{\mathrm{f}}}}{(1-\varphi)+\varphi\dfrac{\rho_{\mathrm{s}}}{\rho_{\mathrm{f}}}}\frac{1}{\mathrm{Re}}\left(\frac{\partial^2\Omega}{\partial X^2}+\frac{\partial^2\Omega}{\partial Y^2}\right)+\left[(1-\varphi)+\varphi\frac{\beta_{\mathrm{s}}}{\beta_{\mathrm{f}}}\right]\frac{\mathrm{Ra}}{\mathrm{Pr}\,\mathrm{Re}^2}\frac{\partial\theta}{\partial X} \tag{11}$$

$$U\frac{\partial\theta}{\partial X}+V\frac{\partial\theta}{\partial Y}=\frac{\dfrac{k_{\mathrm{nf}}}{k_{\mathrm{f}}}}{(1-\varphi)+\varphi\dfrac{(\rho C_{\mathrm{p}})_{\mathrm{s}}}{(\rho C_{\mathrm{p}})_{\mathrm{f}}}}\frac{1}{\mathrm{Re}\,\mathrm{Pr}}\left(\frac{\partial^2\theta}{\partial X^2}+\frac{\partial^2\theta}{\partial Y^2}\right) \tag{12}$$

The additional dimensionless variables in the eqs. (10)-(12) are defined:

$$\Psi=\frac{\psi}{U_mL},\qquad \Omega=\frac{\omega L}{U_m} \tag{13}$$

The dimensionless horizontal and vertical velocities are converted to:

$$U = \frac{\partial \Psi}{\partial Y}, \qquad V = -\frac{\partial \Psi}{\partial X} \tag{14}$$

The appropriate dimensionless boundary conditions can be written:

– on the left wall: $U = V = \Psi = 0, \quad \theta = 1, \text{ and } \Omega = -\dfrac{\partial^2 \Psi}{\partial X^2}$ (15a)

– on the right wall: $U = V = \Psi = 0, \quad \theta = 0, \text{ and } \Omega = -\dfrac{\partial^2 \Psi}{\partial X^2}$ (15b)

– on the top wall: $V = \Psi = 0, \quad U = 1, \quad \dfrac{\partial \theta}{\partial Y} = 0, \text{ and } \Omega = -\dfrac{\partial^2 \Psi}{\partial Y^2}$ (15c)

– on the bottom wall: $U = V = \Psi = 0, \quad \dfrac{\partial \theta}{\partial Y} = 0, \text{ and } \Omega = -\dfrac{\partial^2 \Psi}{\partial Y^2}$ (15d)

In order to estimate the heat transfer enhancement, Nusselt number, Nu(X), and average Nusselt number, $\mathrm{Nu}_{\mathrm{avg}}$, are calculated using eqs. (16) and (17), respectively:

$$\mathrm{Nu}(X) = \frac{k_{\mathrm{nf}}}{k_{\mathrm{f}}} \frac{\partial \theta}{\partial X} \Big|_{X=0} \tag{16}$$

$$\mathrm{Nu}_{\mathrm{avg}} = \int_0^1 \mathrm{Nu}(X)\mathrm{d}Y \tag{17}$$

To evaluate eq. (17), a 1/3 Simpson's rule of integration is implemented. For convenience, a normalized average Nusselt number is defined as the ratio of Nusselt number at any volume fraction of nanoparticles to that of pure water that is [35]:

$$\mathrm{Nu}^*_{\mathrm{avg}}(\varphi) = \frac{\mathrm{Nu}_{\mathrm{avg}}(\varphi)}{\mathrm{Nu}_{\mathrm{avg}}(\varphi = 0)} \tag{18}$$

Variable nanofluid models

What is common in most of the previous referenced work on nanofluid natural and mixed convection problems is the use of the Brinkman [13] viscosity model and Maxwell--Garnett [6] thermal conductivity models for a nanofluid and therefore, predict enhancement of heat transfer due to the presence of nanoparticles. Hence, one of the objectives of this work is to show that a different predictions with using the Pak and Cho [15] viscosity model and Chon *et al.* [12] thermal conductivity model can be obtained, which are shown in the results (only in fig. 15). These correlations are given, respectively:

$$\mu_{\mathrm{nf}} = \mu_{\mathrm{f}}(1 + 39.11\varphi + 533.9\varphi^2) \tag{19}$$

$$\frac{k_{\mathrm{nf}}}{k_{\mathrm{f}}} = 1 + 64.7\varphi^{0.7640} \left(\frac{d_{\mathrm{f}}}{d_{\mathrm{s}}}\right)^{0.3690} \left(\frac{k_{\mathrm{s}}}{k_{\mathrm{f}}}\right)^{0.7476} \mathrm{Pr}_T^{\,0.9955}\, \mathrm{Re}_T^{\,1.2321} \tag{20}$$

where Pr_T and Re_T are defined by:

$$\mathrm{Pr}_T = \frac{\mu_\mathrm{f}}{\rho_\mathrm{f}\alpha_\mathrm{f}} \qquad \text{and} \qquad \mathrm{Re}_T = \frac{\rho_\mathrm{f} k_\mathrm{b} T}{3\pi\mu_\mathrm{f}{}^2 l_\mathrm{f}} \tag{21}$$

The symbol k_b is the Boltzman constant ($1.3807\cdot10^{-23}$ JK^{-1}) and l_f – the mean path of fluid particles given as 0.17 nm [12]. In this model, the temperature and size effects in nanoparticles are considered.

Numerical method

The set of non-linear coupled governing mass, momentum, and energy equations, *i. e.*, eq. (1)-(4), are developed in terms of stream function-vorticity formulation and then solved numerically with the corresponding boundary condition given in eq. (15). The equations are approximated by second-order central difference scheme and successive over relaxation method is used to solve stream function equation. The convergence criterion is defined by the expression:

$$\varepsilon = \frac{\sum_{j=1}^{j=M}\sum_{i=1}^{i=N}\left|\lambda^{n+1}-\lambda^{n}\right|}{\sum_{j=1}^{j=M}\sum_{i=1}^{i=N}\left|\lambda^{n+1}\right|} \le 10^{-6} \tag{22}$$

where ε is the tolerance, M and N are the number of grid points in the X- and Y- direction, respectively. The symbol λ denotes any scalar transport quantity namely Ψ, Ω, or θ. An accurate representation of vorticity at the surface is the most critical step in the stream function–vorticity formulation. A second-order accurate formula is used for the vorticity boundary condition. For example, the vorticity at the top wall is:

$$\Omega_{i,M} = \frac{-\Psi_{i,M} + 8\Psi_{i,M-1} - 7\Psi_{i,M-2} - 6\Delta Y U_m}{2(\Delta Y)^2} \tag{23}$$

The last term in the numerator vanishes for static walls.

Grid testing and code validation

An extensive mesh testing procedure was conducted to guarantee a grid-independent solution. Six different uniform grids, namely, 21 × 21, 41 × 41, 61 × 61, 81 × 81, 101 × 101, and 121 × 121 are employed for the case of Re = 100. The present code was tested for grid independence by calculating the average Nusselt number on the left wall. As it can be observed from fig. 2, an 81 × 81 uniform grid is sufficiently fine to ensure a grid independent solution. Another grid-independence study was performed using Cu-water nanofluid. It was confirmed that the same grid size 81 × 81 ensures a grid-independent solution.

The present numerical solution is further validated by comparing the present code results for temperature distribution at $\mathrm{Ra} = 10^5$ and Pr = 0.70 against the experiment of Krane and Jessee [36] and numerical simulation of Khanafer *et al.* [18] and also Oztop and Abu-Nada [37]. It is clear that the present code is in good agreement with other works reported in literature as shown in fig. 3. In addition the governing equations have been solved for the natural convection flow in an enclosed cavity filled by pure fluid, in order to compare the results

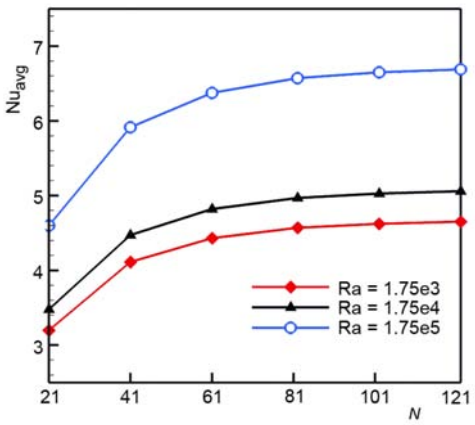

Figure 2. Grid independence study with different Rayleigh number

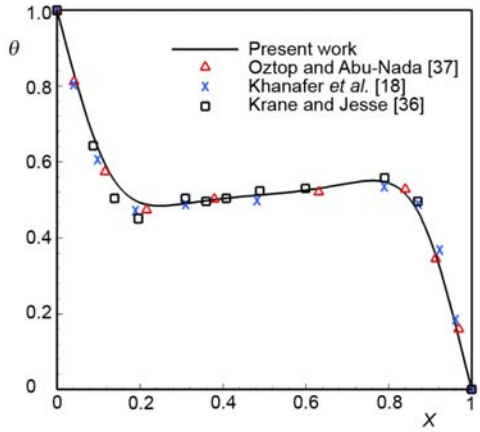

Figure 3. Comparison between present work and other published data for the temperature distribution

with those obtained by Khanafer *et al.* [18], Fusegi *et al.* [38], Markatos and Pericleous [39] and de Vahl Davis [40]. This comparison revealed good agreements between the results, which are shown in tab. 2.

Table 2. Code validation: comparison of the average Nusselt at the top wall

	Present	Khanafer *et al.* [18]	Fusegi *et al.* [38]	Markatos and Pericleous[39]	de Val Davis [40]
$Ra = 10^3$	1.123	1.118	1.052	1.108	1.118
$Ra = 10^4$	2.256	2.245	2.302	2.201	2.243
$Ra = 10^5$	4.521	4.522	4.646	4.430	4.519
$Ra = 10^6$	8.984	8.826	9.012	8.754	8.799

Discussion and results

The 2-D mixed convection is studied in a square lid-driven cavity for $Ra = 1.75 \cdot 10^3$–$1.75 \cdot 10^5$ and solid volume fraction 0 to 0.2 for a Cu-water, TiO_2-water, and Al_2O_3-water nanofluids. Figure 4 illustrates the streamlines at range $Ra = 1.75 \cdot 10^3$ to $1.75 \cdot 10^5$, and Re = 100 for a pure fluid and nanofluid with $\varphi = 10\%$ using Brinkman [10] and Maxwell-Garnett [6] models. Figures 4(a)-(c) show the comparison between TiO_2-water nanofluid (plotted by dashed lines) and pure fluid (plotted by solid lines) on streamlines for various values of the Rayleigh number. At $Ra = 1.75 \cdot 10^3$ (Ri < 1, forced convection-dominated regime), fig. 4(a) indicates that the buoyancy effect is overwhelmed by the mechanical or shear effect due to movement of the top lid and the flow features are similar to those of a viscosity flow of a non-stratified fluid in the lid driven cavity. In this case, the increment of solid concentration does not have considerable effect on the flow pattern. The increase in Rayleigh number enhances the buoyancy effect and therefore the intensity of flow. However, the dominant effect of the force convection is still observed. Furthermore, at $Ra = 1.75 \cdot 10^4$ (Ri = 1, mixed convection-dominated regime), fig. 4(b) indicates that the buoyancy effect is relatively comparable magnitude of the shear effect due to the sliding top wall

lid. In this case, as the solid concentration increases the value of the stream function increases at the center of the cavity. Moreover, for Ra = $1.75 \cdot 10^5$ (Ri > 1, natural convection-dominated regime), fig. 4(c) suggests that the effect of lid-driven flow is insignificant and the value of the stream function increases to a greater extent than previous case as a result of an increase about 10% in the solid concentration. The streamlines for Al_2O_3-water nanofluid and Cu-water nanofluid at various Rayleigh numbers for two case of pure fluid and 10% concentration of nanofluid are presented in figs. 4(d)-(f) and figs. 4(g)-(i), respectively.

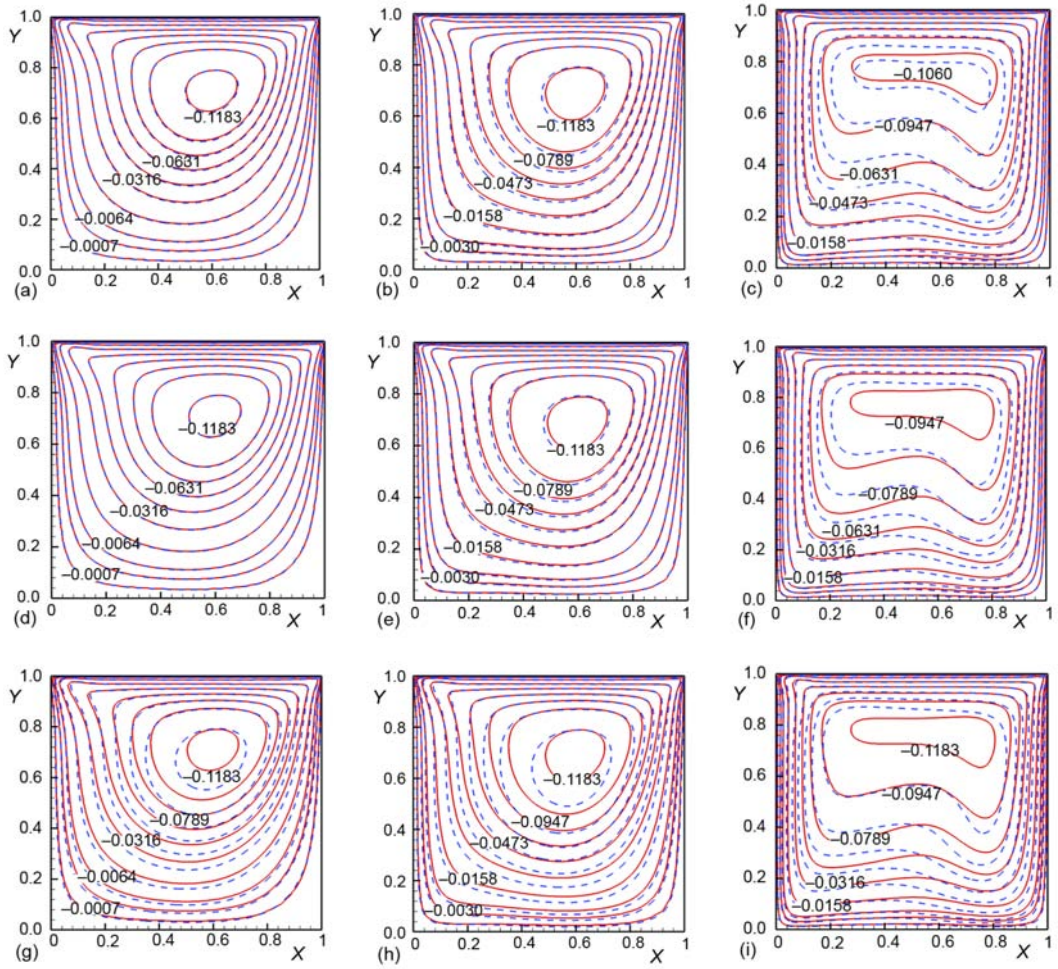

Figure 4. The effect of solid volume fraction, Richardson number and type of nanoparticle on the streamline; (a) TiO_2, Ri = 0.1, (b) TiO_2, Ri = 1, (c) TiO_2, Ri = 10, (d) Al_2O_3, Ri = 0.1, (e) Al_2O_3, Ri = 1, (f) Al_2O_3, Ri = 10, (g) Cu, Ri = 0.1, (h) Cu, Ri = 1, and (i) Cu, Ri = 10; φ = 0%(——), and φ = 10%(-----)

Figures 5(a)-(c) demonstrates the effect of solid concentration on the vertical velocity distribution for various Rayleigh numbers at mid line of cavity (Y = 0.5). It is obvious from this figure that for Ra = $1.75 \cdot 10^3$ the effect of buoyancy predominate the forced convection effect. Upward flow and downward flow are symmetric with respect to the center of the cavity thanks to the laminar behavior of the flow. As seen, the increase in solid concentration

leads to enhance the flow intensity such that the maximum value of the velocity is obtained at the maximum solid concentration. The increase of both Rayleigh number and solid concentration augments the strength of buoyancy. Therefore, the higher Rayleigh number, the solid concentration has more effect to enhance the velocity with respect to the pure fluid. So for TiO_2-water at Ra = $1.75 \cdot 10^3$, the concentration does not effect on the vertical velocity. However, as Ra increases, a mixed effect of buoyancy and lid-driven within the cavity is observed. For instance, at Ra = $1.75 \cdot 10^5$ and 10% solid concentration, the horizontal component of velocity increases by about 8%. Aluminum nanoparticles change from 0% to 10% is the analogous procedure. Due to distinguished thermo-physical properties of Cu, this value can be raised to 25% as shown in fig. 5(i). The effect of the solid concentration on the horizontal velocity distribution for various Rayleigh number at mid-line of the cavity (Y = 0.5) is shown in fig. 6. It turns out that the solid volume fraction increases from 0% to 10% for Cu-water, the horizontal component of velocity increases by almost 20% at Ra = $1.75 \cdot 10^4$, and by about 29% at Ra = $1.75 \cdot 10^5$. Other variations in figs. 6(a)-(i) are significant.

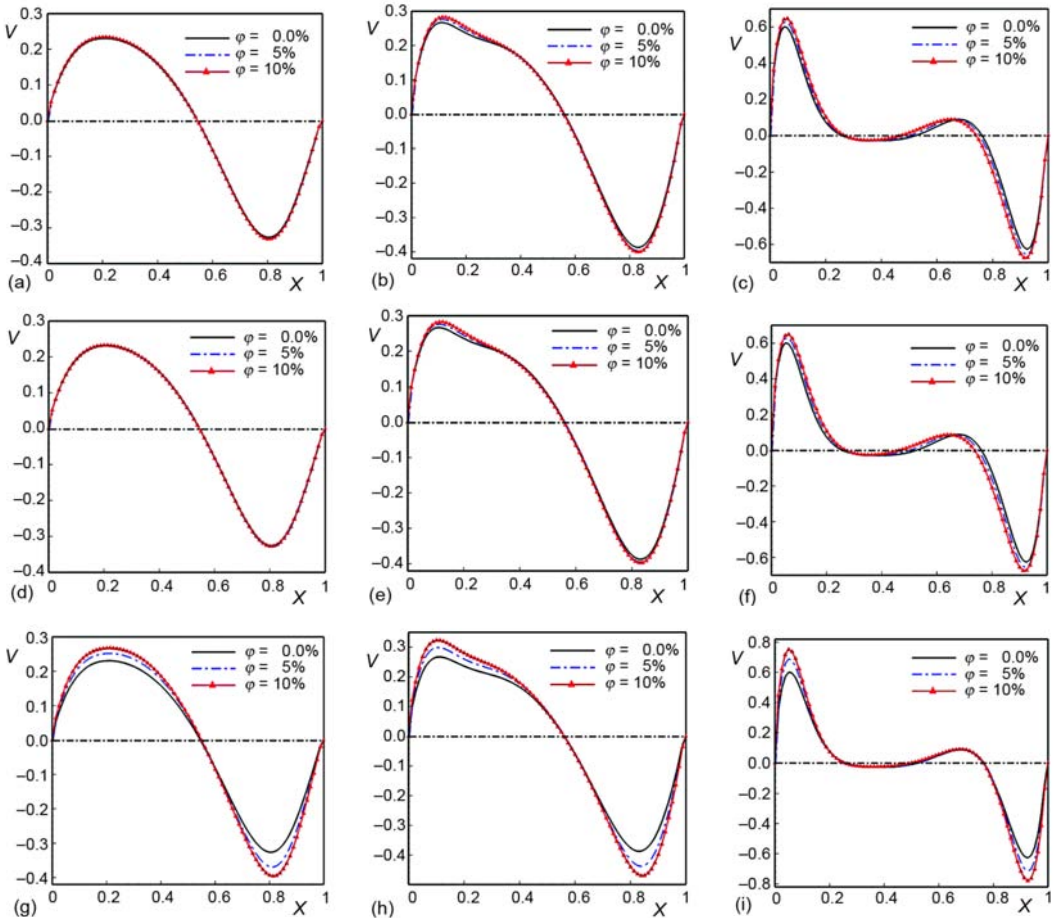

Figure 5. The effect of solid volume fraction, Richardson number, and type of nanoparticle on the vertical velocity at mid line of cavity (Y = 0.5); (a) TiO_2, Ri = 0.1, (b) TiO_2, Ri = 1, (c) TiO_2, Ri = 10, (d) Al_2O_3, Ri = 0.1, (e) Al_2O_3, Ri = 1, (f) Al_2O_3, Ri = 10, (g) Cu, Ri = 0.1, (h) Cu, Ri = 1, and (i) Cu, Ri = 10

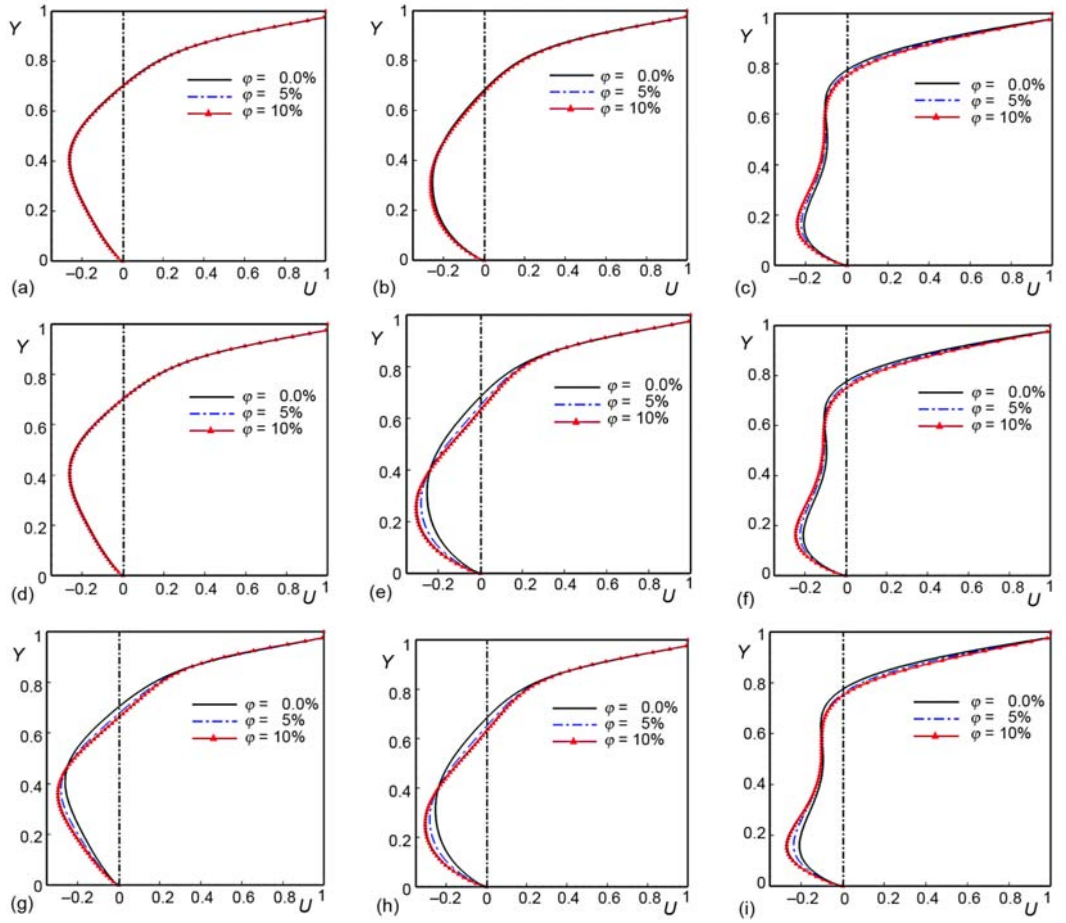

Figure 6. The effect of solid volume fraction, Richardson number and type of nanoparticle on the horizontal velocity at mid line of cavity (X = 0.5) for (a) TiO_2, Ri = 0.1, (b) TiO_2, Ri = 1, (c) TiO_2, Ri = 10, (d) Al_2O_3, Ri = 0.1, (e) Al_2O_3, Ri = 1, (f) Al_2O_3, Ri = 10, (g) Cu, Ri = 0.1, (h) Cu, Ri = 1, (i) Cu, Ri = 10

The effect of the presence of nanoparticle on the thermal behavior and temperature distribution contours for pure water, are overlaid with that for nanofluid with φ of 0.1. The results for Cu-water, Al_2O_3-water, and TiO_2-water at the three Rayleigh number are illustrated in fig. 7. As seen, at the lower Rayleigh number, the solid concentration is more effective to increases the heat penetration because the conduction heat transfer has a stronger contribution at the lower Rayleigh number. On the other hand, the increase of the effective thermal conductivity of the nanofluid with solid concentration leads to enhance the conduction mod. But the effect of conduction heat transfer decreases as the Ra increases. Consequently, at this condition, the solid concentration has a smaller effect on the thermal distribution.

Figures 8, 10, and 12 illustrate the variation of the average Nusselt number on the left wall (hot wall) for TiO_2-water, Al_2O_3-water and Cu-water, respectively. The increase of the solid concentration augments the effective thermal conductivity, and hence, the energy transfer. The increase of the solid concentration also augments the flow intensity. Both of two factors indeed enhance the average Nusselt number with solid concentration. The increase of

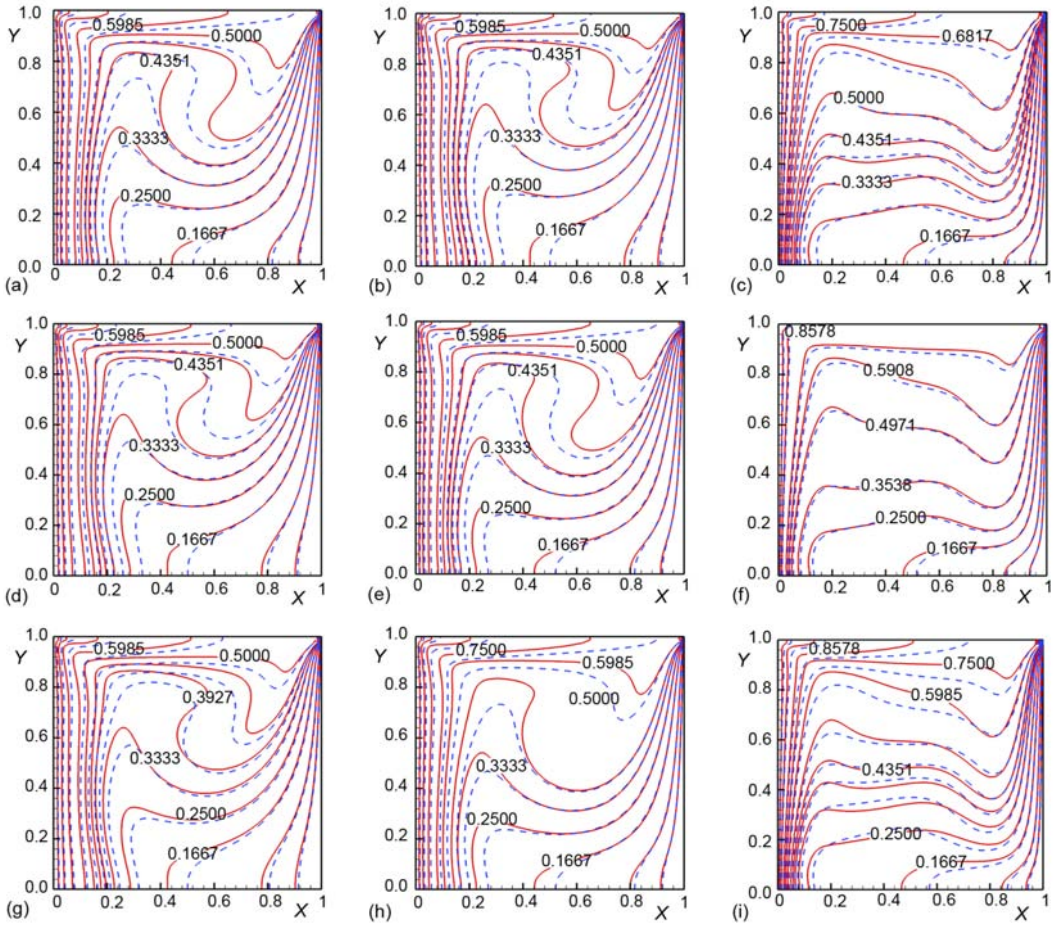

Figure 7. The effect of solid volume fraction, Richardson number, and type of nanoparticle on the isotherms; a) TiO_2, Ri = 0.1, (b) TiO_2, Ri = 1, (c) TiO_2, Ri = 10, (d) Al_2O_3, Ri = 0.1, (e) Al_2O_3, Ri = 1, (f) Al_2O_3, Ri = 10, (g) Cu, Ri = 0.1, (h) Cu, Ri = 1, (i) Cu, Ri = 10; φ = 0% (——), φ = 10% (-----)

Rayleigh number also enhances the heat transfer rate and hence average Nusselt number. It is clear that the solid concentration has more effect on the average Nusselt number at higher Rayleigh number. This is in fact similar to those shown in figs. 5 and 6. Figures 9, 11, and 13 depicts the normalized average Nusselt number Nu^*_{avg} for various values of the volume fraction of nanoparticles φ and Rayleigh number for TiO_2-water, Al_2O_3-water, and Cu-water, respectively. It is observed that as solid volume fraction increases from 0% to 20% at Ra = $1.75 \cdot 10^5$, the Nusselt number increases by about 21% for TiO_2-water, and almost 25% for Al_2O_3-water, and finally around 40% for Cu-water nanofluid. The significance of other variations at different Rayleigh number is shown in fig. 14 in a comparative fashion.

As outlined in fig. 15, it is clear that when Chon *et al.* [12] and Pak and Cho [15] models are used (shown in fig. 15 by Ch-P abbreviation), Nusselt number of the hot wall has higher values at all Rayleigh numbers and φ than that obtained by the Maxwell-Garnett [6] and Brinkman [13] formula, which is shown in fig. 15 by MG-B abbreviation. The differences between the average Nusselt numbers are obtained using the different formulas. Moreover,

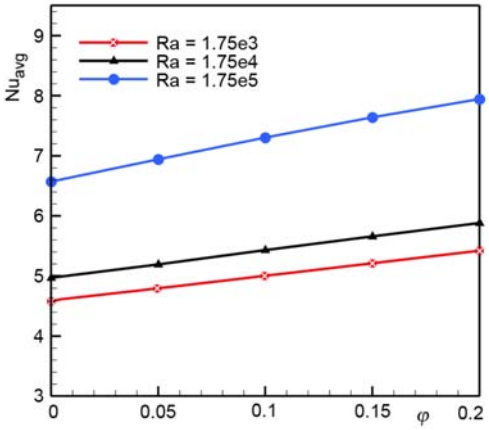

Figure 8. The average Nusselt number at the left wall for TiO_2-water

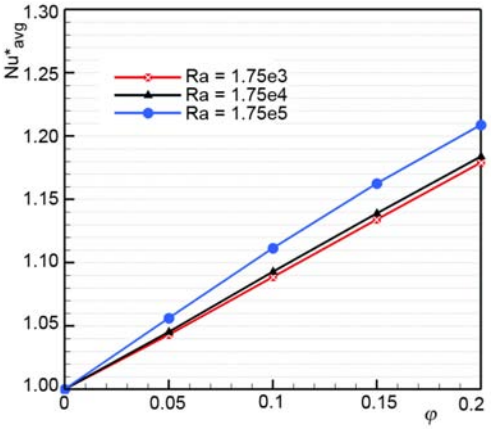

Figure 9. The normalized average Nusselt number at the left wall for TiO_2-water

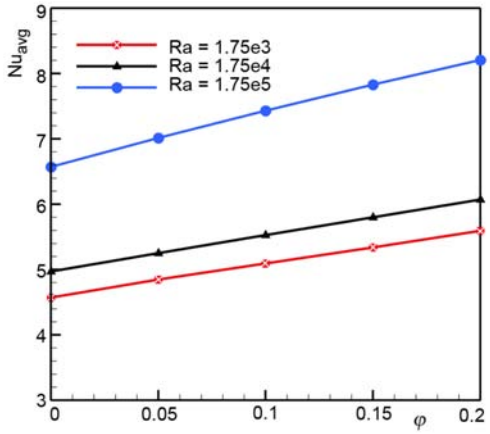

Figure 10. The average Nusselt number at the left wall for Al_2O_3-water

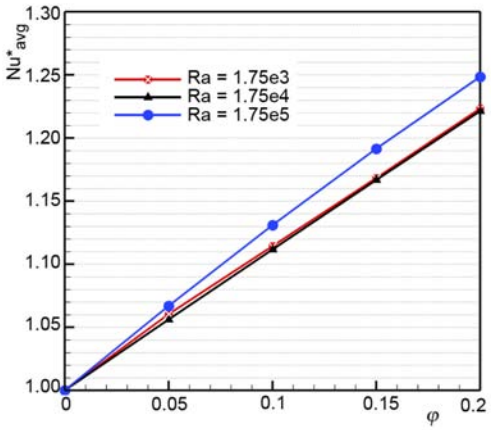

Figure 11. The normalized average Nusselt number at the left wall for Al_2O_3-water

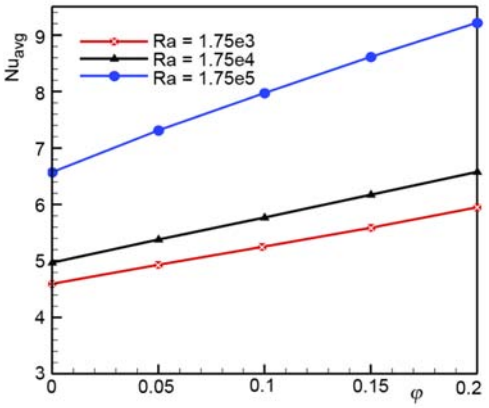

Figure 12. The average Nusselt number at the left wall for Cu-water

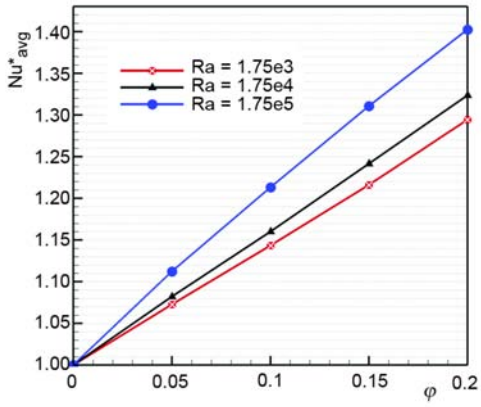

Figure 13. The normalized average Nusselt number at the left wall for Cu-water

a decrease in Rayleigh number results in an increase in the shear force and the forced convection, when a constant nanoparticle volume-fraction utilized, and this causes the difference between average Nusselt numbers calculated by two combinations of formula to increase. It is recognized from fig. 15, when the Maxwell-Garnett [6] and Brinkman [12] formula are used, the heat transfer increases with increasing solid volume fraction and the average Nusselt number has an irregular manner when Chon *et al.* [13] and Pak and Cho [15] correlations are utilized. It is found that at low Rayleigh number the average Nusselt number is more sensitive to viscosity models and thermal conductivity models.

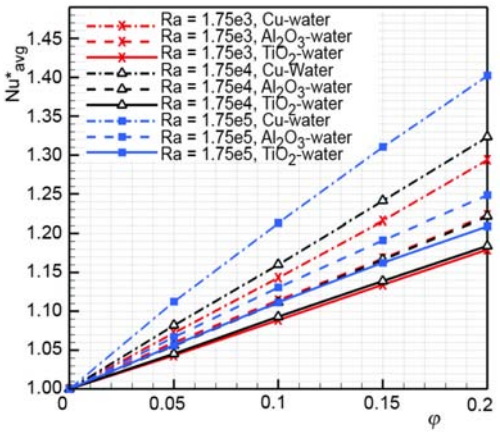

Figure 14. The normalized average Nusselt number in various solid concentration and Rayleigh number; effect of type of nanofluid

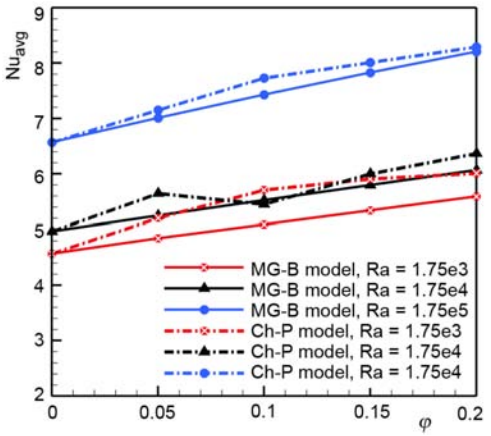

Figure 15. The average Nusselt number in various solid concentrations and Rayleigh number; effect of nanofluid model for Al_2O_3-water

Conclusions

A numerical study has been performed to investigate the effect of using different nanofluids on mixed convection flow field and temperature distributions in lid-driven square cavity from the left vertical hot wall using Maxwell-Garnet [6] thermal conductivity and Brinkman [13] viscosity models. The top and bottom walls of the cavity are kept insulated and the top wall moved to the right at the constant speed. The important conclusions drawn as the following:

- Increasing the value of Rayleigh number and volume fraction of nanoparticles enhances the heat transfer keeping other parameters fixed.
- The type of nanofluid is a key factor to heat transfer enhancement. The highest values are obtained when using Cu nanoparticles.
- For assumed Reynolds number, the increase in the solid concentration augments the stream-function, also *U* and *V*-component of velocity, particularly at the higher Rayleigh number.
- It was recognized that at low Rayleigh numbers, Nu_{avg} was more sensitive to the viscosity and the thermal conductivity models.

Present research is confined to study of two viscosity models and two thermal conductivity models for Al_2O_3-water nanofluid. Anyway, the results show that the utilized model, apart from the type of nanoparticle, can be effective on heat transfer enhancement.

In the future, the study can be extended for more thermal conductivity models, viscosity models and different Reynolds number. An optimization study may be necessary for this work to find out the best model which has most compatibility with experimental results for cavity configuration.

Nomenclature

C_p – specific heat at constant pressure, [Jkg^{-1}K^{-1}]
g – gravitational acceleration, [ms^{-2}]
Gr – Grashof number (= g$\beta(T_H - T_C)L^3\nu_f^{-2}$), [–]
k – thermal conductivity, [Wm^{-1}K^{-1}]
k_b – Boltzmann′s constant (= 1.38065·10^{-23})
L – length of cavity, [m]
Nu – Nusselt number (= hL/k_f), [–]
P – dimensionless pressure (= $p\rho_{nf}^{-1}U_m^{-2}$), [–]
p – dimensional pressure, [kgm^{-1}s^{-2}]
Pr – Prandtl number (= ν_f/α_f), [–]
Ra – Rayleigh number (= GrPr), [–]
Re – Reynolds number (= U_mL/ν_f), [–]
Ri – Richardson number (= Gr/Re^2), [–]
T – dimensional temperature, [°C]
u, v – dimensional x and y components of velocity, [ms^{-1}]
U, V – dimensionless velocities ($V = v/U_m$, $U = u/U_m$), [–]
U_m – lid velocity, [m s^{-1}]
x, y – dimensional co-ordinates, [m]
X, Y – dimensionless co-ordinates ($X = x/L$, $Y = y/L$), [–]

Greek symbols

α – fluid thermal diffusivity, [m^{2}s^{-1}]
β – thermal expansion coefficient, [K^{-1}]
ε – numerical tolerance, [–]
φ – nanoparticle volume fraction, [–]
ν – kinematic viscosity, [m^{2}s^{-1}]
θ – dimensionless temperature, $(T - T_C)/(T_H - T_C)$, [–]
λ – transport quantity
ψ – dimensional stream function, [m^{2}s^{-1}]
Ψ – dimensionless stream function (= ψ/U_mL), [–]
ω – dimensional vorticity [s^{-1}]
Ω – dimensionless vorticity (= $\omega L/U_m$), [–]
ρ – density, [kgm^{-3}]
μ – dynamic viscosity, [Nsm^{-2}]

Subscripts

avg – average
f – fluid
H – hot
C – cold
nf – nanofluid
s – solid particle

Superscripts

* – normalized

References

[1] Godson, L., *et al.*, Enhancement of Heat Transfer Using Nanofluids – an Overview, *Renewable Sustainable Energy Rev. 14* (2010), 2, pp. 629-641
[2] Eastman, J. A., *et al.*, Enhanced Thermal Conductivity through the Development of Nanofluids, *Proceedings*, Nanophase and Nanocomposite Materials II, MRS, Pittsburg, Penn., USA (eds., S., Komarneni, J. C., Parker, H. J., Wollenberger) (1997), Vol. 497, pp. 3-11
[3] Lee, S., *et al.*, Measuring Thermal Conductivity of Fluids Containing Oxide Nanoparticles, *Heat and Mass Transfer 121* (1999), 2, pp. 280-289
[4] Das, S. K., *et al.*, Temperature Dependence of Thermal Conductivity Enhancement for Nanofluids, *Trans. ASME, Heat Transfer 125* (2003), 4, pp. 567-574
[5] Maxwell, J. C., *A Treatise on Electricity and Magnetism*, Second ed., Oxford University Press, Cambridge, UK, (1904), pp. 435-441
[6] Maxwell-Garnett, J. C., Colours in Metal Glasses and in Metallic Films, *Philos. Trans. R. Soc. A 203* (1904), pp. 385-420
[7] Bruggeman, D. A. G., Calculation of Various Physical Constants of Heterogeneous Substances (in German), *Ann. Physik. Leipzig, 24* (1935), pp. 636-679
[8] Hamilton, R. L., Crosser, O. K., Thermal Conductivity of Heterogeneous Two Component Systems, *I & EC, Fundamentals 1* (1962), 3, pp. 182-191
[9] Wasp, F. J., *Solid-Liquid Flow Slurry Pipeline Transportation*, Trans. Tech. Publ., Berlin, 1977
[10] Yu, W., Choi, S. U. S., The Role of Interfacial Layers in the Enhanced Thermal Conductivity of Nanofluids: a Renovated Maxwell Model, *Nanopart. Res. 5* (2003), 1-2, pp. 167-171

[11] Patel, H. E., *et al.*, A Micro Convection Model for Thermal Conductivity of Nanofluid, *Pramana-Journal of Physics 65* (2005), 5, pp. 863-869
[12] Chon, C. H., *et al.*, Empirical Correlation Finding the Role of Temperature and Particle Size for Nanofluid (Al_2O_3) Thermal Conductivity Enhancement, *Appl. Phys. Lett. 87* (2005), 15, pp. 153107-153107-3
[13] Brinkman, H. C., The Viscosity of Concentrated Suspensions and Solution, *J. Chem. Phys. 20* (1952), 4, pp. 571-581
[14] Nguyen, C. T., *et al.*, Temperature and Particle Size Dependent Viscosity Data for Water based Nanofluids Hysteresis Phenomenon, *Int. J. Heat Fluid Flow 28* (2007), 6, pp. 1492-1506
[15] Pak, B. C., Cho, Y., Hydrodynamic and Heat Transfer Study of Dispersed Fluids with Submicron Metallic Oxide Particle, *Exp. Heat Transfer 11* (1998), 2, pp. 151-170
[16] Jang, S. P., Choi, S. U. S., The Role of Brownian Motion in the Enhanced Thermal Conductivity of Nanofluids, *Appl. Phys. Lett. 84* (2004), 21, pp. 4316-4318
[17] Chang, H., Rheology of CuO Nanoparticle Suspension Prepared by ASNSS, *Reviews on Advanced Materials Science 10* (2005), 2, pp. 128-132
[18] Khanafer, K., *et al*., Buoyancy Driven Heat Transfer Enhancement in a Two-Dimensional Enclosure Utilizing Nanofluids, *Int. J. Heat Mass Transfer 46* (2003), 19, pp. 3639-3653
[19] Oztop, H. F., Dagtekin, I., Mixed Convection in Two-Sided Lid-Driven Differentially Heated Square Cavity, *Int. J. Heat Mass Transfer 47* (2004), 8-9, pp. 1761-1769
[20] Cheng, T. S., Characteristics of Mixed Convection Heat Transfer in a Lid-Driven Square Cavity with Various Richardson and Prandtl Numbers, *International Journal of Thermal Sciences 50* (2011), 2, pp. 197-205
[21] Tiwari, R. K., Das, M. K., Heat Transfer Augmentation in a Two-Sided Lid-Driven Differentially Heated Square Cavity Utilizing Nanofluids, *Int. J. Heat Mass Transfer 50* (2007), 9-10, pp. 2002-2018
[22] Sebdania, S. M., *et al*., Effect of Nanofluid Variable Properties on Mixed Convection in a Square Cavity, *International Journal of Thermal Sciences 52* (2012), 1, pp. 112-126
[23] Ouertatani, N., *et al.*, Mixed Convection in a Double Lid-Driven Cubic Cavity, *Int. J. Therm. Sci. 48* (2009), 7, pp. 1265-1272
[24] Arpaci, V. S., Larsen, P. S., Convection Heat Transfer, Prentice-Hall, Inc., Upper Saddle River, N. J., USA, 1984
[25] Torrance, K., *et al.*, Cavity Flows Driven by Buoyancy and Shear, *J. Fluid Mech. 51* (1972), 2, pp. 221-231
[26] Iwatsu, R., *et al*., Mixed Convection in a Driven Cavity with a Stable Vertical Temperature Gradient, *Int. J. Heat Mass Transfer 36* (1993), 6, pp. 1601-1608
[27] Ramanan, N., Homsy, G. M., Linear Stability of Lid-Driven Cavity Flow, *Phys. Fluids 6* (1994), 8, pp. 2690-2701
[28] Iwatsu, R., *et al*., Convection in a Differentially-Heated Square Cavity with a Torsionally-Oscillating Lid, *Int. J. Heat Mass Transfer 35* (1992), 5, pp. 1069-1076
[29] Iwatsu, R., *et al*., Numerical Simulation of Flows Driven by a Torsionally Oscillating Lid in a Square Cavity, *J. Fluids Eng. 114* (1992), 2, pp. 143-149
[30] Oztop, H. F., Dagtekin, I., Mixed Convection in Two-Sided Lid-Driven Differentially Heated Square Cavity, *International Journal of Heat and Mass Transfer 47* (2004), 8-9, pp. 1761-1769
[31] Chamkha A. J., Abu-Nada, E., Mixed Convection Flow in Single and Double-Lid Driven Square Cavities Filled with Water-Al_2O_3 Nanofluid: Effect of Viscosity Models, *European Journal of Mechanics-B/Fluid, 36* (2012), Nov.-Dec., pp. 82-96
[32] Talebi, F., *et al*., Numerical Study of Mixed Convection Flows in a Square Lid-Driven Cavity Utilizing Nanofluid, *International Communications in Heat and mass Transfer, 37* (2010), 1, pp. 79-90
[33] Muthtamilselvan, M., *et al*., Heat Transfer Enhancement of Copper-Water Nanofluids in a Lid-Driven Enclosure, *Commun. Nonlinear Sci. Numer. Simul. 15* (2010), 6, pp. 1501-1510
[34] Xuan, Y., Li, Q., Investigation on Convective Heat Transfer and Flow Features of Nanofluids, *ASME J. Heat Transfer 125* (2003), 1, pp. 151-155
[35] Abu-Nada, E., Effects of Variable Viscosity and Thermal Conductivity of CuO-Water Nanofluid on Heat Transfer Enhancement in Natural Convection: Mathematical Model and Simulation, *J. Heat Transfer 132* (2010), 5, pp. 052401

[36] Krane, R. J., Jessee, J., Some Detailed Field Measurements for a Natural Convection Flow in a Vertical Square Enclosure, *Proceedings*, First ASMEJSME Thermal Engineering Joint Conference, Tokyo, (1983), Vol. 1, pp. 323-329
[37] Oztop, H. F., Abu-Nada, E., Numerical Study of Natural Convection in Partially Heated Rectangular Enclosures Filled with Nanofluids, *International Journal of Heat and Fluid Flow 29* (2008), 5, pp. 1326-1336
[38] Fusegi, T., *et al*., A Numerical Study of Three Dimensional Natural Convection in a Differentially Heated Cubic Enclosure, *Int. J. Heat Mass Transfer 34* (1991), 6, pp. 1543-1557
[39] Markatos, N. C., Pericleous, K. A., Laminar and Turbulent Natural Convection in an Enclosed Cavity, *Int. J. Heat Mass Transfer, 27* (1984), 5, pp. 755-772
[40] G. de Vahl Davis, Natural Convection of Air in a Square Cavity: a Benchmark Solution, *Int. J. Numer. Methods Fluids, 3* (1983), 3, pp. 249-264

Paper submitted: July 15, 2012
Paper revised: May 14, 2013
Paper accepted: May 14, 2013